A mathematical model of doxorubicin penetration through multicellular layers

C.J. Evans, R.M. Phillips, P.F. Jones, P.M. Loadman, B.D. Sleeman, C.J. Twelves, S.W. Smye

www.elsevier.com/locate/yjtbi

A mathematical model of doxorubicin penetration through multicellular layers

C.J. Evans, R.M. Phillips, P.F. Jones, P.M. Loadman, B.D. Sleeman, C.J. Twelves, S.W. Smye

PII: S0022-5193(08)00604-8
DOI: doi:10.1016/j.jtbi.2008.11.031
Reference: YJTBI5369

To appear in: *Journal of Theoretical Biology*

Received date: 15 August 2008
Revised date: 14 November 2008
Accepted date: 17 November 2008

Cite this article as: C.J. Evans, R.M. Phillips, P.F. Jones, P.M. Loadman, B.D. Sleeman, C.J. Twelves and S.W. Smye, A mathematical model of doxorubicin penetration through multicellular layers, *Journal of Theoretical Biology* (2009), doi:10.1016/j.jtbi.2008.11.031

A mathematical model of doxorubicin penetration through multicellular layers

C.J. Evans[a,*], R.M. Phillips[b], P.F Jones[c], P.M. Loadman[b], B.D. Sleeman[d], C.J. Twelves[e], S.W. Smye[a,f]

[a]Division of Medical Physics, Leeds Institute of Genetics, Health and Therapeutics, University of Leeds, LS2 9JT, United Kingdom

[b]Institute of Cancer Therapeutics, University of Bradford, Bradford, BD7 1DP, United Kingdom

[c]Section of Molecular Gastroenterology, Leeds Institute of Molecular Medicine, University of Leeds, St James's University Hospital, Leeds, LS9 7TF, United Kingdom

[d]Department of Applied Mathematics, University of Leeds, Leeds, LS2 9JT, United Kingdom

[e]Section of Oncology and Clinical Research, Leeds Institute of Molecular Medicine, University of Leeds, St James's University Hospital, Leeds, LS9 7TF, United Kingdom

[f]Department of Medical Physics and Engineering, Leeds Teaching Hospitals, St James's University Hospital, Leeds, LS9 7TF, United Kingdom

*Corresponding author. Medical Physics and Engineering, Level 1 Bexley Wing, St James's University Hospital, Leeds, LS9 7TF. Tel. +44 113 2067841. Fax: +44 113 2068941

E-mail address: c.j.evans@leeds.ac.uk

Abstract

Inadequate drug delivery to tumours is now recognised as a key factor that limits the efficacy of anticancer drugs. Extravasation and penetration of therapeutic agents through avascular tissue are critically important processes if sufficient drug is to be delivered to be therapeutic. The purpose of this study is to develop an in silico model that will simulate the transport of the clinically-used cytotoxic drug doxorubicin across multicell layers (MCLs) *in vitro*. Three cell lines were employed: DLD-1 (human colon carcinoma), MCF7 (human breast carcinoma) and NCI/ADR-Res (doxorubicin resistant and P-glycoprotein [Pgp] overexpressing ovarian cell line). Cells were cultured on transwell culture inserts to various thicknesses and doxorubicin at various concentrations (100 or 50 μM) was added to the top chamber. The concentration of drug appearing in the bottom chamber was determined as a function of time by HPLC-MS/MS. The rate of drug penetration was inversely proportional to the thickness of the multicell layer. The rate and extent of doxorubicin penetration was no different in the presence of NCI/ADR-Res cells expressing Pgp compared to MCF7 cells. A mathematical model based upon the premise that the transport of doxorubicin across cell membrane bilayers occurs by a passive "flip-flop" mechanism of the drug between two membrane leaflets was constructed. The mathematical model treats the transwell apparatus as a series of compartments and the multicell layer is treated as a series of cell layers, separated by small intercellular spaces. This model demonstrates good agreement between predicted and actual drug penetration *in vitro* and may be applied to the prediction of drug transport *in vivo*, potentially becoming a useful tool in the study of optimal chemotherapy regimes.

Keywords: Drug transport; P-glycoprotein; chemotherapy; theoretical model

Introduction

Both acquired and inherent resistance to cytotoxic and targeted anticancer agents are typically associated with biochemical or molecular changes at the cellular level. These include decreased drug uptake, increased drug efflux via extrusion pumps such as P-Glycoprotein (Pgp), reduced target expression, direct mutation of the molecular target and increased repair of DNA damage . Whilst these undoubtedly contribute to drug resistance, impaired drug delivery to tumours or 'pharmacokinetic drug resistance' is also recognised as a significant barrier to effective drug treatment . Seminal studies conducted in the late 1970's using multicell spheroids *in vitro* clearly demonstrated that significant drug penetration barriers exist for clinically important anticancer drugs such as doxorubicin . This comparatively simple experimental model provided the first indication that the failure of many solid tumours to respond to chemotherapy could be due to insufficient drug being delivered to the tumour. The factors that determine how much drug is delivered to the tumours are complex, but include the drug's pharmacokinetic profile, elevated interstitial pressure in tumours, the chaotic and inefficient nature of the blood supply to tumours and strong binding of drugs to cellular and extracellular macromolecules .

The development of *in silico* models that can forecast the movement of drugs through tumours may provide tools for optimising drug delivery. A quantitative understanding of drug delivery to tumour cells requires a mathematical framework to describe the dynamics of how drugs get to and penetrate through the tumour mass. In the first instance, a basic model is required in order that key mechanisms influencing drug delivery can be identified and characterised. The experimental multicell layer (MCL)

model, initially developed by Cowan et al. (1996) and modified by Phillips et al. (1998) fulfils this criterion (figure 1). Cell layers are grown in a controlled manner to various thicknesses on a microporous membrane and the drug added to the top chamber. The concentration of drug appearing in the bottom chamber can be determined as a function of time using chromatographic techniques.

The aim of this work was to develop a mathematical model for drug transport through MCLs for doxorubicin, an anthracycline cytotoxic drug used widely in the treatment of patients with cancer. Doxorubicin was selected for several reasons; first, previous studies have shown that tissue penetration is an issue with doxorubicin. Secondly, doxorubicin transport into and out of cells and extravascular transport through MCLs have been modelled mathematically. These models are limited as they are primarily focused on drugs whose penetration through MCLs is diffusion-limited; they do however serve as a basis for the current study. Finally, doxorubicin also has the advantage of being naturally fluorescent so is easily detectable by chromatographic techniques and fluorescence microscopy.

Methods

Cell culture and drug penetration

A schematic of the experimental apparatus is shown in figure 1A. It consists of a transwell insert placed into one well of a 24 well plate. Cells are grown on a collagen coated membrane (0.4 μm pore size) that separates the top from the bottom chamber. The thickness of the multicell layer can be varied (figure 1B) by adjusting incubation time post-seeding. The membrane itself is 50 μm thick and is 6.5 mm in diameter. The

cells have an average diameter of approximately 25 μm so there are around 70,000 cells in a layer one cell thick.

Three cell lines were used in this study: DLD1 (human colon carcinoma), MCF7 (human breast carcinoma) and NCI/ADR-Res (doxorubicin resistant OVCAR8 cells). Resistance of NCI/ADR-Res cells to doxorubicin was confirmed prior to drug penetration. IC50 values measure the effectiveness of a compound in inhibiting biochemical function and represent the concentration of a drug required for 50% inhibition *in vitro*. Following 1 hour exposure to doxorubicin, IC50 values of >100 μM, 1.05 ± 0.67 μM and 2.20 ± 0.78 μM were obtained for the NCI/ADR-Res, MCF7 and DLD1 cells respectively. Cells were routinely maintained in RPMI 1640 culture medium supplemented with 10% foetal calf serum, sodium pyruvate (2mM), L-glutamine (2 mM) and buffered with HEPES (25 mM). Phenol red free medium was used for drug penetration studies, to prevent interference with doxorubicin peaks on HPLC chromatograms. MCLs which had been cultured for 1, 3 and 5 days were analysed for each cell line, in parallel with no cell controls. The thickness of the MCL was determined by microscopic analysis of histological cross sections using a graduated eyepiece which had been calibrated using a stage micrometer.

Doxorubicin (at 50 or 100 μM) was added initially (as bolus) to the top chamber and the concentration of drug reaching the bottom chamber was determined as a function of time by high pressure liquid chromatography (HPLC) with mass spectrometry (MS) detection. The bottom chamber was constantly stirred. Samples, each of 10 μl, were taken from the bottom chamber every 2 minutes for the first 10 minutes, then every 5

minutes subsequently. At each time point, 10 µl of fresh media was added to the bottom chamber such that the volume in the bottom chamber remained constant at 600 µl.

HPLC analysis of Doxorubicin.

High purity HPLC grade solvents (Fisher Scientific, Loughborough, UK), analytical grade chemicals (Sigma Chemical Co. Ltd. Poole, UK) and triple distilled water were used throughout. Each 10 µl sample taken for analysis was added to 290 µl of fresh culture medium and doxorubicin, extracted by solid phase extraction (SPE). Each SPE cartridge C18-(EC), 50 mg, was primed by adding 1 ml methanol followed by 1ml of 0.02% formic acid into the cartridge. The analytical sample (300 µl) was added to each cartridge which was washed by adding 1 ml of 0.02% formic acid solution, then dried under vacuum. Doxorubicin was eluted from the cartridge using 1.5 ml isopropanol:methanol (3:1) and the eluent evaporated to dryness in a centrifugal evaporator at room temperature. The sample was reconstituted in 30 µl of mobile phase A and transferred to polypropylene vials for injection into the HPLC.

Chromatographic analysis of doxorubicin used mobile phase A comprising 90% 5 mM ammonium formate, adjusted to pH 3.5 with formic acid, 10% acetonitrile and mobile phase B comprising 40 % 5 mM ammonium formate, adjusted to pH 3.5 with formic acid, 60% acetonitrile. The mobile phases were mixed in a ratio of 60% A to 40% B. Separation was achieved using a Waters C18 10cm Acquity column (1.7 µm x 2.1 mm: Milford, MA, USA) with a mobile phase flow rate of 0.4 ml/min was used. Samples were injected (5 µl) using a Waters Acquity Separation Module and the total run time was 3 minutes. Detection was performed using a Waters Quattro Premier MS/MS in

parallel with diode array UV-vis absorbance detection. MS detection of doxorubicin utilised a Multiple Reaction Monitoring (MRM) channel extracted at 544.04 > 396.9 *m/z*. in ES+ mode. Capillary voltage was set to 3.75 kV, cone 22 V, source temperature 100 degrees C, desolvation temperature 300 C and collision energy 12V. The MRM dwell was 0.2 seconds. The limit of quantification for this method of detection was 2 nM doxorubicin. Calibration curves were established by spiking tissue culture medium (300 µl) with a range of doxorubicin concentrations (0-50 nM): samples ere extracted and analysed as described above.

Biological basis of the mathematical model

Figure 2 is a schematic of the transport of doxorubicin in and out of MDR-type cells, based on the work of Eytan (2005) who considered the case of a single cell contained within a pool of drug. Our model develops from that to consider doxorubicin transport through multicellular layers. Doxorubicin in the extracellular medium is adsorbed (represented by the rate constant k_4) into the outer leaflet of the plasma membrane. The reverse process is represented by k_{-4}. Drug bound to the membrane then undergoes a "flip-flop" process (k_1) in which it is transferred from the outer to the inner leaflet and vice-versa. Doxorubicin in the inner leaflet is rapidly released from (k_5) and can rebind to (k_{-5}) the cytoplasm. Once inside the cell, drug can bind (k_2) to molecular sinks in the nucleus, such as DNA, and also be extruded directly out into the extracellular space via Pgp (k_p).

The rates of adsorption and desorption of the drug present in the cell membrane are sufficiently fast that drug in the outer membrane is in practical equilibrium with the

drug pool in the extracellular medium . Similarly, drug in the inner membrane is in equilibrium with the pool in the cytoplasm. For this reason, the mathematical model neglects these processes, assuming the flip-flop (k_1) to be the rate-limiting step.

The histology of the MCLs seen in figure 1B shows that the cell lines considered in this work are tightly packed, so it is reasonable to assume that all drug transport between top and bottom chambers (in the presence of cells) is via the mechanism shown above, i.e. there is no leakage.

Mathematical model

The mathematical model treats the transwell apparatus as a series of compartments, shown in figure 3. The MCL is treated as a series of cell layers, separated by small intercellular spaces. The number of layers used in the model is determined by the duration of incubation used to grow the MCL. Typically, layers incubated for 1, 3 and 5 days are approximately 1, 2 and 3 cells thick respectively. The collagen-coated membrane is treated as a compartment in its own right.

It is assumed that all cells contain a given concentration of sites to which doxorubicin can bind. The model allows doxorubicin within the cell layers to bind to these sites until no free sites remain. Drug can also dissociate itself, becoming free within the cell layer once again and also making its binding site available. Since doxorubicin can also bind within the Transwell membrane, a similar process to represent this is included in the model.

The Pgp pumping can be modelled by Michaelis-Menten type kinetics (Eytan and Kuchel, 1999) and its pump activity in typical Pgp overexpressing cells is estimated to be around 1-50 nmoles / second / 10^9 cells (Eytan, 2005). Transport rates associated with the binding of doxorubicin within the cell and membrane layers are assumed to be proportional to the product of the concentration of free drug and the concentration of free binding sites. The transport rate between all other compartments is assumed to be proportional to concentration in the originating compartment.

Suppose n cell layers are present. We denote the concentration of drug (μM) in compartment j by C_j, as shown in figure 3.

The parameters used in the model are shown in table 1, which also shows the values of those parameters which are known or estimated at the outset. The values of r_2, r_{-2}, r_3 and r_{-3} will largely depend on the rates of the reactions by which doxorubicin binds to DNA or to sites in the collagen-coated membrane. These rates have been assigned nominal values on the assumption that they will be significantly larger than the other transport rates (Eytan and Kuchel, 1999) and therefore their exact values will not greatly affect the overall rate of drug penetration since the flip-flop process will always be the rate-limiting step. Dissociation rates (r_{-2} and r_{-3}) were assumed to be a tenth of their respective binding rates, following Eytan (2005). V_L and V_I were estimated by examining microscopic histology images such as those shown in figure 1B.

The concentrations in each compartment over time are then defined by the following system of ODEs, using the nomenclature of figure 3.

For the top chamber compartment:

$$V_T \frac{dC_T}{dt} = -r_1 C_T + r_1 C_{L1} + \frac{r_p C_{L1}}{2(k_m + C_{L1})}$$

The LHS of this equation is the rate of change of the amount of doxorubicin in the top chamber. The first term on the RHS corresponds to drug being lost (at a rate r_1) from the top chamber into the first cell layer, and the second term is the reverse process. The third term is the Michaelis-Menten term associated with the Pgp pump extruding doxorubicin from the first cell layer back into the top chamber.

The next compartment holds the free drug in the first cell layer:

$$V_L \frac{dC_{L1}}{dt} = r_1 C_T + r_1 C_{I1} - 2r_1 C_{L1} - \frac{r_p C_{L1}}{(k_m + C_{L1})} - r_2 C_{L1}(C_0 - C_{b1}) + r_{-2} C_{b1}$$

Here, the first three terms represent the passive transport of drug between the first cell layer and its neighbouring compartments (the top chamber and the first intercellular layer). The fourth term is drug being lost from the compartment due to the Pgp pump. Free drug in this layer can also be lost due to binding at a rate proportional to the concentration of free drug multiplied by the concentration of free binding sites. This process is modelled in the fifth term, while the sixth term represents bound doxorubicin being released back into the compartment.

The remainder of the equations are derived similarly and are shown below:

$$V_{\mathrm{L}}\frac{dC_{b1}}{dt} = r_2 C_{L1}(C_0 - C_{b1}) - r_{-2}C_{b1}$$

$$V_I\frac{dC_{I1}}{dt} = -2r_1 C_{I1} + r_1 C_{L1} + r_1 C_{L2} + \frac{r_p C_{L1}}{2(k_m + C_{L1})} + \frac{r_p C_{L2}}{2(k_m + C_{L2})}$$

$$\left.\begin{aligned} V_L\frac{dC_{Li}}{dt} &= r_1 C_{I(i-1)} + r_1 C_{Ii} - 2r_1 C_{Li} - \frac{r_p C_{Li}}{(k_m + C_{Li})} - r_2 C_{Li}(C_0 - C_{bi}) + r_{-2}C_{bi} \\ V_{\mathrm{L}}\frac{dC_{bi}}{dt} &= r_2 C_{Li}(C_0 - C_{bi}) - r_{-2}C_{bi} \\ V_I\frac{dC_{Ii}}{dt} &= -2r_1 C_{Ii} + r_1 C_{Li} + r_1 C_{L(i+1)} + \frac{r_p C_{Li}}{2(r_m + C_{Li})} + \frac{r_p C_{L(i+1)}}{2(r_m + C_{L(i+1)})} \end{aligned}\right\} i = 2,\ldots,n-1$$

$$V_{\mathrm{L}}\frac{dC_{Ln}}{dt} = r_1 C_{I(n-1)} + r_1 C_{In} - 2r_1 C_{Ln} - \frac{r_p C_{Ln}}{(k_m + C_{Ln})} - r_2 C_{Ln}(C_0 - C_{bn}) + r_{-2}C_{bn}$$

$$V_{\mathrm{L}}\frac{dC_{bn}}{dt} = r_2 C_{Ln}(C_0 - C_{bn}) - r_{-2}C_{bn}$$

$$V_I\frac{dC_{In}}{dt} = -r_1 C_{In} - r_0 C_{In} + r_1 C_{Ln} + r_0 C_M + \frac{r_p C_{Ln}}{2(k_m + C_{Ln})}$$

$$V_{\mathrm{M}}\frac{dC_M}{dt} = -2r_0 C_M + r_0 C_{In} + r_0 C_B - r_3 C_M(M_0 - C_{bM}) + r_{-3}C_{bM}$$

$$V_{\mathrm{M}}\frac{dC_{bM}}{dt} = r_3 C_M(M_0 - C_{bM}) - r_{-3}C_{bM}$$

$$V_{\mathrm{B}}\frac{dC_B}{dt} = -r_0 C_B + r_0 C_M$$

The ODEs are subject to the initial conditions:

$$C_T(0) = T_0$$
$$C_{Li}(0) = C_{bi}(0) = C_{Ii}(0) = 0 \qquad i = 1,\ldots,n$$
$$C_M(0) = C_{bM}(0) = C_B(0) = 0$$

This system has one realistic (non-negative) steady state given by:

$$C_T = C_{Ii} = C_M = C_B = \phi \qquad i = 1,\ldots,n$$
$$C_{Li} = \varphi \qquad i = 1,\ldots,n$$
$$C_{bi} = \frac{r_2 C_0}{r_{-2} + r_2\varphi} \qquad i = 1,\ldots,n$$
$$C_{bM} = \frac{r_3 M_0}{r_{-3} + r_3\phi} \qquad i = 1,\ldots,n$$

where ϕ and φ satisfy:

$$\phi V_T + \phi V_M + C_{bM} V_M + \phi V_B + n(V_L \varphi + V_L C_{bi} + V_I \varphi) = T_0 V_T$$
$$2r_1 \varphi^2 + (2r_1 k_m + r_p - 2r_1 \phi)\varphi - 2r_1 k_m \phi = 0$$

In the absence of the Pgp pump ($r_p=0$), we have $\varphi=\phi$.

Note that if $r_p=0$ and also $r_{-3} << r_3$ and $r_{-2} << r_2$ (in other words the dissociation of doxorubicin is much slower then its binding) the steady state solution can be written down concisely and becomes

$$\phi(V_T + V_M + V_B + nV_I + nV_L) + M_0 V_M + nC_0 V_L \approx T_0 V_T$$
$$\phi \approx \frac{T_0 V_T - M_0 V_M - nC_0 V_L}{V_T + V_M + V_B + nV_L + nV_I}$$

which is intuitively reasonable.

We can non-dimensionalise the above system as follows, switching to a long time scale.

$$\tau = \frac{r_1}{V_T} t$$
$$z_T = \frac{1}{T_0} C_T, z_{Li} = \frac{1}{T_0} C_{Li}, z_{bi} = \frac{1}{C_0} C_{bi}, z_{Ii} = \frac{1}{T_0} C_{Ii} \qquad i = 1, \ldots, n$$
$$z_M = \frac{1}{T_0} C_M, z_{bM} = \frac{1}{M_0} C_{bM}, z_B = \frac{1}{T_0} C_B$$
$$\alpha_0 = \frac{r_0}{r_1}, \alpha_2 = \frac{r_2 C_0}{r_1}, \beta_2 = \frac{r_{-2}}{r_2 T_0}, \alpha_3 = \frac{r_3 M_0}{r_1}, \beta_3 = \frac{r_{-3}}{r_3 T_0}, \alpha_p = \frac{r_p}{r_1 T_0}, \alpha_m = \frac{k_m}{T_0}$$
$$W_L = \frac{V_T}{V_L}, W_I = \frac{V_T}{V_I}, W_M = \frac{V_T}{V_M}, W_B = \frac{V_T}{V_B}$$

The resulting system of equations is as follows:

$$\frac{dz_T}{d\tau} = -z_T + z_{L1} + \frac{\alpha_p z_{L1}}{2(\alpha_m + z_{L1})}$$

$$\frac{1}{W_L}\frac{dz_{L1}}{d\tau} = z_T + z_{I1} - 2z_{L1} - \frac{\alpha_p z_{L1}}{(\alpha_m + z_{L1})} - \alpha_2 z_{L1}(1 - z_{b1}) + \alpha_2 \beta_2 z_{b1}$$

$$\frac{1}{W_{\mathrm{L}}}\frac{dz_{b1}}{d\tau} = \alpha_2 z_{L1}(1 - z_{b1}) - \alpha_2 \beta_2 z_{b1}$$

$$\frac{1}{W_I}\frac{dz_{I1}}{d\tau} = -2z_{I1} + z_{L1} + z_{L2} + \frac{\alpha_p z_{L1}}{2(\alpha_m + z_{L1})} + \frac{\alpha_p z_{L2}}{2(z_m + z_{L2})}$$

$$\left.\begin{aligned} \frac{1}{W_L}\frac{dz_{Li}}{d\tau} &= z_{I(i-1)} + z_{Ii} - 2z_{Li} - \frac{\alpha_p z_{Li}}{(\alpha_m + z_{Li})} - \alpha_2 z_{Li}(1 - z_{bi}) + \alpha_2 \beta_2 z_{bi} \\ \frac{1}{W_L}\frac{dz_{bi}}{d\tau} &= \alpha_2 z_{Li}(1 - z_{bi}) - \alpha_2 \beta_2 z_{bi} \\ \frac{1}{W_I}\frac{dz_{Ii}}{d\tau} &= -2z_{Ii} + z_{Li} + z_{L(i+1)} + \frac{\alpha_p z_{Li}}{2(\alpha_m + z_{Li})} + \frac{\alpha_p z_{L(i+1)}}{2(\alpha_m + z_{L(i+1)})} \end{aligned}\right\} i = 2, \ldots, n-1$$

$$\frac{1}{W_L}\frac{dz_{Ln}}{d\tau} = z_{I(n-1)} + z_{In} - 2z_{Ln} - \frac{\alpha_p z_{Ln}}{(\alpha_m + z_{Ln})} - \alpha_2 z_{Ln}(1 - z_{bn}) + \alpha_2 \beta_2 z_{bn}$$

$$\frac{1}{W_{\mathrm{L}}}\frac{dz_{bn}}{d\tau} = \alpha_2 z_{Ln}(1 - z_{bn}) - \alpha_2 \beta_2 z_{bn}$$

$$\frac{1}{W_I}\frac{dz_{In}}{d\tau} = -z_{In} - \alpha_0 z_{In} + z_{Ln} + \alpha_0 z_M + \frac{\alpha_p z_{Ln}}{2(\alpha_m + z_{Ln})}$$

$$\frac{1}{W_{\mathrm{M}}}\frac{dz_M}{d\tau} = -2\alpha_0 z_M + \alpha_0 z_{In} + \alpha_0 z_B - \alpha_3 z_M(1 - z_{bM}) + \alpha_3 \beta_3 z_{bM}$$

$$\frac{1}{W_{\mathrm{M}}}\frac{dz_{bM}}{d\tau} = \alpha_3 z_M(1 - z_{bM}) - \alpha_3 \beta_3 z_{bM}$$

$$\frac{1}{W_{\mathrm{B}}}\frac{dz_B}{d\tau} = -\alpha_0 z_B + \alpha_0 z_M$$

The approximate non-dimensional parameter values are given below.

$W_L \approx 200, W_I \approx 1000, W_M \approx 60, W_B \approx 0.2$

$\alpha_0 \approx 1.3, \alpha_p \approx 10^{-4}, \alpha_m \approx 50$

$T_0 = 100$

$\alpha_2, \alpha_3 \approx 10^5$

$\beta_2, \beta_3 \approx 10^{-3}$

It can be seen from these values that, over this time scale, the terms corresponding to the Pgp pump are small in comparison to others since k_p is small. Also, since $1/W_L$, $1/W_I$ and $1/W_C$ are all small, the left hand sides of the ODEs involving these terms are small.

Approximate solution

If we accept the approximations above (α_p, $1/W_L$, $1/W_I$, $1/W_C \approx 0$) thereby neglecting the Pgp pump, then we can reduce the system to two differential equations and a system of linear equations:

$$\frac{dz_T}{d\tau} = -z_T + z_{L1}$$
$$0 = z_T + z_{I1} - 2z_{L1}$$
$$0 = -2z_{I1} + z_{L1} + z_{L2}$$
$$\left.\begin{aligned} 0 &= z_{I(i-1)} + z_{Ii} - 2z_{Li} \\ 0 &= -2z_{Ii} + z_{Li} + z_{L(i+1)} \end{aligned}\right\} \quad i = 2, \ldots, n-1 \qquad (n \geq 3)$$
$$0 = z_{I(n-1)} + z_{In} - 2z_{Ln}$$
$$0 = -z_{In} - \alpha_0 z_{In} + z_{Ln} + \alpha_0 z_M$$
$$0 = -2\alpha_0 z_M + \alpha_0 z_{In} + \alpha_0 z_B$$
$$\frac{1}{W_B}\frac{dz_B}{d\tau} = -\alpha_0 z_B + \alpha_0 z_M$$

The set of $2n+1$ linear equations can now be solved for z_{Li}, z_{Ii} and z_C in terms of z_T and z_B. This solution is as follows:

$$z_{Lj} = \frac{z_T(2n\alpha_0 - 2j\alpha_0 + 2 + \alpha_0) + (2j\alpha_0 - \alpha_0)z_B}{2(1+n\alpha_0)}$$
$$z_{Ij} = \frac{z_T(n\alpha_0 - j\alpha_0 + 1) + j\alpha_0 z_B}{(1+n\alpha_0)}$$
$$z_M = \frac{z_T + (1+2n\alpha_0)z_B}{2(1+n\alpha_0)}$$

$$\frac{dz_T}{d\tau} = \frac{\alpha_0}{2(1+n\alpha_0)}(z_B - z_T) = -\frac{1}{W_B}\frac{dz_B}{d\tau}$$

which leads to the final solutions

$$z_T(\tau) = \frac{1}{1+W_B}(W_B + e^{-\omega_n(1+W_B)\tau})$$

$$z_B(\tau) = \frac{W_B}{1+W_B}(1 - e^{-\omega_n(1+W_B)\tau})$$

$$\omega_n = \frac{\alpha_0}{2(1+n\alpha_0)}$$

In dimensional terms, this is

$$C_T(t) \approx \frac{T_0 V_B}{V_T + V_B}(\frac{V_T}{V_B} + e^{-\Omega t})$$

$$C_B(t) \approx \frac{T_0 V_T}{V_T + V_B}(1 - e^{-\Omega t})$$

$$\Omega = \frac{r_0 r_1 (V_T + V_B)}{2V_T V_B (r_1 + nr_0)}$$

If the quantity of drug bound in the cell and collagen layers is significant, a better approximation to C_B is given by:

$$C_B(t) \approx \frac{V_T T_0 - nV_L C_0 - V_M M_0}{V_T + V_B}(1 - e^{-\Omega t})$$

Figure 4 shows the full and approximate model solutions for one cell layer with varying values of T_0.

Pharmacokinetic drug input

Suppose that rather than having a top chamber that contains an initial concentration of drug which then transfers through the system, the concentration of drug at the input to the system is a function of time, $p_k(t)$. This is closer to the situation *in vivo* in which drug concentration in the vasculature follows a known pharmacokinetic profile in time.

In this case, the ODE corresponding to the top chamber is discarded and the equation for C_{L1} becomes:

$$V_{\mathrm{L}}\frac{dC_{L1}}{dt} = r_1 p_k(t) + r_1 C_{I1} - 2r_1 C_{L1} - \frac{r_p C_{L1}}{(k_m + C_{L1})} - r_2 C_{L1}(C_0 - C_{b1}) + r_{-2} C_{b1}$$

If we suppose that $p_k(t)=T_0 p(\tau)$, with $p(0)=1$, then we can non-dimensionalise as before. If the previous approximations remain valid, the long time-scale approximate solution is:

$$z_{Lj} \approx \frac{p(\tau)(2n\alpha_0 - 2j\alpha_0 + 2 + \alpha_0) + (2j\alpha_0 - \alpha_0)z_B}{2(1+n\alpha_0)}$$

$$z_{Ij} \approx \frac{p(\tau)(n\alpha_0 - j\alpha_0 + 1) + j\alpha_0 z_B}{(1+n\alpha_0)}$$

$$z_M \approx \frac{p(\tau) + (1+2n\alpha_0)z_B}{2(1+n\alpha_0)}$$

and

$$-\frac{1}{W_B}\frac{dz_B}{d\tau} = \frac{\alpha_0}{2(1+n\alpha_0)}(z_B - p(\tau))$$

$$\mathrm{A}p(\tau) = \frac{dz_B}{d\tau} + \mathrm{A}z_B, \quad \mathrm{A} = \frac{\alpha_0 W_B}{2(1+n\alpha_0)}$$

The solution to this ODE is given by

$$z_B(\tau) = e^{-\mathrm{A}\tau}\left(const + \mathrm{A}\int e^{\mathrm{A}\tau} p(\tau)d\tau\right)$$

If $p(\tau)$ is a typical PK profile of the form $p(\tau) = \sum_{i=1}^{m} \varepsilon_i e^{-\delta_i \tau}$ and $z_B(0)=0$, then

$$z_B(\tau) \approx \mathrm{A}\left(\sum_{i=1}^{m} \frac{\varepsilon_i}{\mathrm{A} - \delta_i}(e^{-\delta_i \tau} - e^{-A\tau})\right)$$

Note that $\dot{z}_B(0) > 0$, and $z_B(\tau) = 0$ for some $\tau > 0$ only if $\delta_i > \mathrm{A}$ for some i.

It follows from the expressions for the approximate cell concentrations and from z_B that the *j*th cell layer concentration is of the form

$$z_{Lj}(\tau) = \left(\sum_{i=1}^{m} \lambda_{ij} e^{-\delta_i \tau} \right) - \lambda_{0j} e^{-\mathrm{A}\tau}$$

for some constants $\lambda_{0j},\ldots, \lambda_{mj}$ (see below)

The area under the concentration-time curve for the *j*th cell layer is therefore given by

$$T_0 \int_0^{\infty} z_{Lj}(\tau) d\tau = T_0 \left(\sum_{i=1}^{m} \left(\lambda_{ij} \int_0^{\infty} e^{-\delta_i \tau} d\tau \right) - \lambda_0 \int_0^{\infty} e^{-\mathrm{A}\tau} d\tau \right)$$

$$T_0 \int_0^{\infty} z_{Lj}(\tau) d\tau = T_0 \left(\sum_{i=1}^{m} \frac{\lambda_{ij}}{\delta_i} - \frac{\lambda_0}{\mathrm{A}} \right)$$

where the constants λ_{ij} are given by

$$\lambda_{ij} = \varepsilon_i \left(1 + \frac{\omega_n \delta_i (2j-1)}{(\omega_n W_B - \delta_i)} \right)$$

$$\lambda_{0j} = \omega_n^2 W_B (2j-1) \sum_{i=1}^{m} \frac{\varepsilon_i}{\omega_n W_B - \delta_i}$$

and

$$\omega_n = \frac{\alpha_0}{2(1+n\alpha_0)}$$

Results

Concentrations of doxorubicin over time were measured in the bottom chamber of the transwell experiments in the absence of cells following addition of 50 and 100 μM doxorubicin (figure 5); for each of the cell lines after addition of 50 (figure 6) and 100 μM doxorubicin (figure 7). The measured concentrations of doxorubicin in the top and bottom chambers are shown in figure 8 after addition of 50 and 100 μM doxorubicin.

Experiments were also performed using 25 μM doxorubicin (figure 8). In the presence of cells, however, typical bottom chamber concentrations on day 5 were often below 1-2 ng/ml (2 μM) which is lower than the analytical limit of quantitation. For this reason, these data were not considered in the analysis below.

The 100 μM control experiments (figure 5), along with weighted least squares curve-fitting techniques, were used to determine the value of the model parameters r_0 as 0.13 μl/s and M_0 as 200 μM.

Three cell lines were used, DLD1, MCF7 and the drug resistant NCI/ADR-Res, in which substantially more active extrusion takes place. MCLs cultured for 1, 3 and 5 days were generated. The approximate thicknesses of the resulting cell layers are shown in table 2.

The penetration curves for the MCF7 and NCI/ADR-Res cells were very similar and generally within experimental error of each other (figure 9). This is consistent with the prediction of the model that realistic values of r_p will mean that pump terms are small in comparison with other transport mechanisms.

Values of r_1 and C_0 were determined for each cell line by fitting model predictions to the 100 μM measured data, since these data were less subject to experimental error. The resulting values were r_1=0.1 μl/s for DLD1 and r_1=0.05 μl/s for both MCF7 and NCI/ADR-Res; C_0=200 μM in all cases.

Using these parameter values, the model predictions of bottom chamber doxorubicin concentrations, after addition of 100 μM doxorubicin to the top chamber, were determined for the differing MCL thicknesses of MCF7 (figure 10) and DLD-1 cells (figure 11). There was a high level of concordance in all cases between the concentrations measured *in vitro* and those calculated using the model *in silico*. Note that the predictions shown in these graphs are those of the full mathematical model, not the long time-scale approximation.

Discussion

Drawing on Eytan's previous work (Eytan, 2005), we have developed a novel model for the transport of doxorubicin through MCLs performed initial validation using a Transwell system described above. This model has several important advantages over existing models; first, it incorporates pharmacokinetic data reflecting the changing concentration of drug in a blood vessel supplying a tumour over time. Secondly, the model previously developed by Eytan addressed doxorubicin transport into and out of cells rather than across a MCL which is more representative of a tumour. Finally, Hicks et al. (1997) have described a model for extravascular transport of drugs through MCLs; this process is diffusion-limited which is not the case for some drugs including doxorubicin (see below).

The current model treats the system as a group of compartments, including a series of cell layers, which are assumed to be well mixed on the time scales at which drug moves between them. The processes of drug transport through cell layers in our model are based on the biological mechanisms associated with movement of doxorubicin in drug-

resistant cells as previously described. Pgp substrates such as doxorubicin cross cell membranes by distinct flip-flop events rather than by diffusion (Tunggal et al, 2000). Doxorubicin dwells in the outer membrane leaflet for on average 0.7min (Regev et al., 2005) and this is likely to be a limiting factor where cells are tightly packed. Because doxorubicin inhibits DNA and RNA synthesis by intercalating between base pairs, for the purpose of examining drug distribution it effectively binds inside cell nuclei. The model incorporates all of these characteristics.

The model parameters r_0, r_1, M_0 and C_0 were used to fit model predictions to the experimental data, and it was possible to achieve generally good agreement between the two, although the measurements were subject to significant experimental uncertainty. The effect of ATP dependent drug transporters, such as the Pgp pump on drug penetration, has been debated and potentially competing processes have been identified. Interestingly, in this study we found no significant difference in the bottom chamber concentrations of doxorubicin between the Transwell experiments with MCF7 and NCI/ADR-Res MCLs. Eytan makes a quantitative estimate of the pumping activity of drug-resistant cells that suggests the quantity of drug transported in this way would be small by comparison with the other processes taking place. It is possible, however, that with smaller quantities of drug in the system, the pump may play a more significant role.

When the amount of drug in the system is large compared to the quantity of binding sites, it is possible to solve the mathematical system analytically to achieve an approximate solution for the concentration in all compartments over a prolonged time

scale. In this situation, the concentration of drug in a given compartment over time depends linearly on T_0 and all available binding sites will be occupied in a short period of time. However, the more interesting and clinically relevant situation is one in which the number of binding sites is comparable to the amount of drug in the system. In this case, the approximate solution is not valid, and the proportion of binding sites occupied in a given layer over the course of a PK drug input depends nonlinearly on T_0 and the number of cell layers present. Given that the anthracyclines and many other cytotoxics must intercalate DNA or RNA to be effective, this information is potentially of great clinical relevance to optimising chemotherapeutic regimes in cases where penetration of drug into the tumour is an important factor in cellular resistance.

The model has several potential uses. In early pre-clinical development, it could be incorporated in the process of lead optimisation so that tissue penetration becomes one of the criteria for selecting which one out of a series of potential therapeutics is taken into detailed *in vivo* evaluation. Potentially more important, however, is the ability of such a model to predict the extent of drug penetration clinically under conditions that cannot be achieved in the Transwell. For example, it is possible to simulate *in silico* MCLs more than 3-4 cells thick, which are difficult to achieve *in vitro.* Likewise, our *in vitro* experiments used initial doxorubicin concentrations of 50 and 100 μM to allow easier detection of drug in the bottom chamber. Such concentrations are not physiologically achievable, but the mathematical model allows estimation of penetration at more clinically relevant concentrations. In mice and humans, peak plasma concentrations of doxorubicin following IV injection can be as high as 30 μg/ml though typical values are between 1 and 10 μg/ml (Loadman et al, 1999). These translate to

peak values of around 60 μM and typical values of 2-20 μM. As described in the results, experiments performed with 25 μM doxorubicin result in typical bottom chamber concentrations of 1-2 ng/ml (2 nM) which, given a sample of 10 μl, are lower than the analytical limit of quantitation. While the model has therefore not been verified at these lower concentrations, it is assumed that it can be used to extrapolate to these situations.

Finally, whereas the *in vitro* model has a fixed concentration of drug initially in the top chamber, the *in silico* model can predict doxorubicin distribution across MCLs over a period of time as the pharmacokinetic profile of the drug under evaluation changes.

Acknowledgements

This work was supported by a pump priming grant from Yorkshire Cancer Research

References

Arpino, G., Wiechmann, L., Osborne, C.K., and Schiff, R., 2008. Crosstalk between the estrogen receptor and the HER tyrosine kinase receptor family: molecular mechanism and clinical implications for endocrine therapy resistance. Endocr Rev 29, 217-33.

Chien, A.J., and Moasser, M.M., 2008. Cellular mechanisms of resistance to anthracyclines and taxanes in cancer: intrinsic and acquired. Semin Oncol 35, S1-S14; quiz S39.

Cowan, D.S., Hicks, K.O., and Wilson, W.R., 1996. Multicellular membranes as an in vitro model for extravascular diffusion in tumours. Br J Cancer Suppl 27, S28-31.

Eytan, G.D. and Kuchel, P.W., 1999. Mechanism of action of P-glycoprotein in relation to passive membrane permeation. Int. Rev. Cytol. 190:175-250.

Eytan, G.D., 2005. Mechanism of multidrug resistance in relation to passive membrane permeation. Biomed Pharmacother 59, 90-7.

Grantab, R., Sivananthan, S., and Tannock, I.F., 2006. The penetration of anticancer drugs through tumor tissue as a function of cellular adhesion and packing density of tumor cells. Cancer Res 66, 1033-9.

Heldin, C.H., Rubin, K., Pietras, K., and Ostman, A., 2004. High interstitial fluid pressure - an obstacle in cancer therapy. Nat Rev Cancer 4, 806-13.

Hicks, K.O., Ohms, S.J., van Zijl, P.L., Denny, W.A., Hunter, P.J., and Wilson, W.R., 1997. An experimental and mathematical model for the extravascular transport of a DNA intercalator in tumours. Br J Cancer 76, 894-903.

Kelley, M.R., and Fishel, M.L., 2008. DNA repair proteins as molecular targets for cancer therapeutics. Anticancer Agents Med Chem 8, 417-25.

Lemos, C., Jansen, G., and Peters, G.J., 2008. Drug transporters: recent advances concerning BCRP and tyrosine kinase inhibitors. Br J Cancer 98, 857-62.

Loadman, P.M., Bibby, M.C., Double J.A., Al-Shakhaa, W.M., and Duncan, R, 1999. Pharmacokinetics of PK1 and doxorubicin in experimental colon tumor models with differing responses to PK1. Clin Cancer Res 5, 3682-2688.

Minchinton, A.I., and Tannock, I.F., 2006. Drug penetration in solid tumours. Nat Rev Cancer 6, 583-92.

Phillips, R.M., Loadman, P.M., and Cronin, B.P., 1998. Evaluation of a novel in vitro assay for assessing drug penetration into avascular regions of tumours. Br J Cancer 77, 2112-9.

Regev, R., and Eytan, G.D., 1997. Flip-flop of doxorubicin across erythrocyte and lipid membranes. Biochem Pharmacol 54, 1151-8.

Regev, R., Yeheskely-Hayon, D., Katzir, H. and Eytan, G.D., 2005. Transport of anthracyclines and mitoxantrone across membranes by a flip-flop mechanism. Biochem. Pharmacol 70, 161-9.

Scudiero, D.A., Monks, A., and Sausville, E.A., 1998. Cell line designation change: multidrug-resistant cell line in the NCI anticancer screen. J Natl Cancer Inst 90, 862.

Sutherland, R.M., Eddy, H.A., Bareham, B., Reich, K., and Vanantwerp, D., 1979. Resistance to adriamycin in multicellular spheroids. Int J Radiat Oncol Biol Phys 5, 1225-30.

Tannock, I.F., Lee, C.M., Tunggal, J.K., Cowan, D.S., and Egorin, M.J., 2002. Limited penetration of anticancer drugs through tumor tissue: a potential cause of resistance of solid tumors to chemotherapy. Clin Cancer Res 8, 878-84.

Tunggal, J.K., Cowan, D.S., Shaikh, H., and Tannock, I.F., 1999. Penetration of anticancer drugs through solid tissue: a factor that limits the effectiveness of chemotherapy for solid tumors. Clin Cancer Res 5, 1583-6.

Tunggal, J.K., Melo, T., Ballinger, J.R., and Tannock, I.F., 2000. The influence of expression of P-glycoprotein on the penetration of anticancer drugs through multicellular layers. Int J Cancer 86, 101-7.

Figure legends

Figure 1. The experimental Transwell setup (A) and histology of DLD-1 multicell layers (B) ranging from 20 μm to 85 μm thick . The scale bar in figure 1B equals 50 μm.

Figure 2. Transport mechanisms of doxorubicin in MDR-type cells, adapted from Eytan.

Figure 3. Schematic of the compartmental setup and transport mechanisms for the mathematical model with two cell layers present. The nomenclature for doxorubicin concentrations in each compartment is also shown.

Figure 4. Comparison of full and approximate model solutions. One cell layer present, with parameter values as given elsewhere for the DLD1 cell line.

Figure 5. Bottom chamber measurements. Control experiments (no cells present). Each value represents the mean ± standard deviation for three independent experiments.

Figure 6. Bottom chamber measurements of doxorubicin concentration for three cell lines with initial top chamber concentration of T_0=50μM

Figure 7. Bottom chamber measurements of doxorubicin concentration for three cell lines with initial top chamber concentration of T_0=100μM.

Figure 8. Bottom chamber measurements of doxorubicin concentration in DLD1 cells with initial top chamber concentration of T_0=25μM.

Figure 9. Comparison of bottom chamber measurements of doxorubicin concentration between MCF7 (solid lines) and NCI/ADR-Res (dotted lines), for initial top chamber concentrations of 50 and 100 μM.

Figure 10. Comparison of modelled (dotted lines) and measured (solid lines) bottom chamber doxorubicin concentrations. MCF7 cell line with initial top chamber concentration of T_0=100μM

Figure 11. Comparison of modelled (dotted lines) and measured (solid lines) bottom chamber doxorubicin concentrations. DLD1 cell line with initial top chamber concentration of T_0=100μM

Figure 12. Comparison of modelled (dotted lines) and measured (solid lines) bottom chamber doxorubicin concentrations. MCF7 cell line with initial top chamber concentration of T_0=50μM

Figure 13. Comparison of modelled (dotted lines) and measured (solid lines) bottom chamber doxorubicin concentrations. DLD1 cell line with initial top chamber concentration of T_0=50μM

Table legends

Table 1. Model parameters and their meaning with known and estimated values where applicable.

Table 2. Approximate thicknesses of multicellular layers for each cell line. Measurements are in μm.

Table 1

Parameter	Meaning	Value	Source
r_0	Rate of transport to/from membrane	n/a	to be determined experimentally
r_1	Rate of transport to/from cell layer	n/a	to be determined experimentally
r_2	Rates of transport due to	100 µl µM^{-1}s^{-1}	nominal value
r_{-2}	binding/dissociation within cell layer	10 µl s^{-1}	nominal value
r_3	Rates of transport due to	100 µl µM^{-1}s^{-1}	nominal value
r_{-3}	binding/dissociation within membrane	10 µl s^{-1}	nominal value
r_p	Maximum transport rate due to Pgp pumping	0.0035 µmol s^{-1}	Eytan, 2005
k_m	Michaelis constant associated with Pgp pumping	2.0 µM	Eytan, 2005
V_T	Volume of top chamber	100 µl	known
V_L	Volume of cell layers	0.8 µl	estimated from histology
V_I	Volume of intermediate layers	0.05 µl	estimated from histology
V_M	Volume of membrane	1.65 µl	known
V_B	Volume of bottom chamber	600 µl	known
C_0	Initial concentration of free binding sites in cell layer	n/a	to be determined experimentally
M_0	Initial concentration of free binding sites in membrane	n/a	To be determined experimentally

Table 2.

Day	MCF7	NCI/ADR-Res	DLD-1
1	24.6 ± 6.4	21.4 ± 4.4	18.4 ± 7.4
3	37.4 ± 8.1	35.6 ± 7.8	29.6 ± 10.1
5	46.2 ± 4.3	45.1 ± 9.2	37.4 ± 5.6

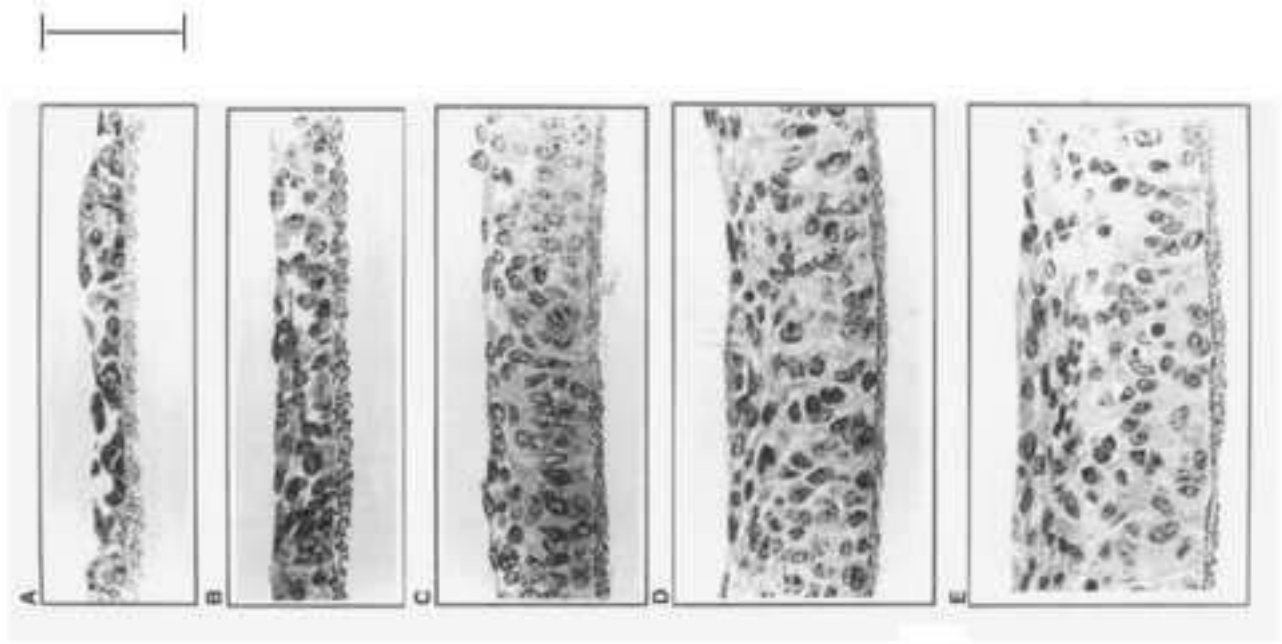
A
B
C
D
E

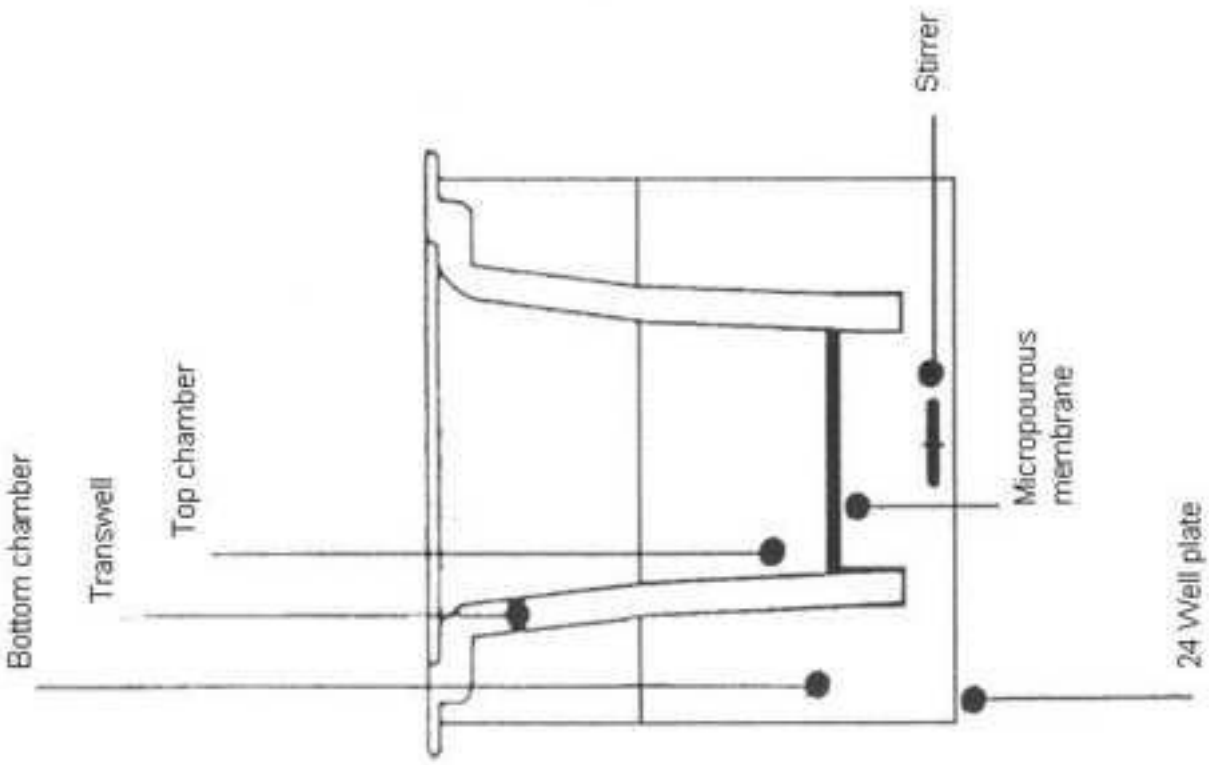
Bottom chamber
Transwell
Top chamber
Stirrer
Micropourous membrane
24 Well plate

4. Figure 1

4. Figure 2

4. Figure 3

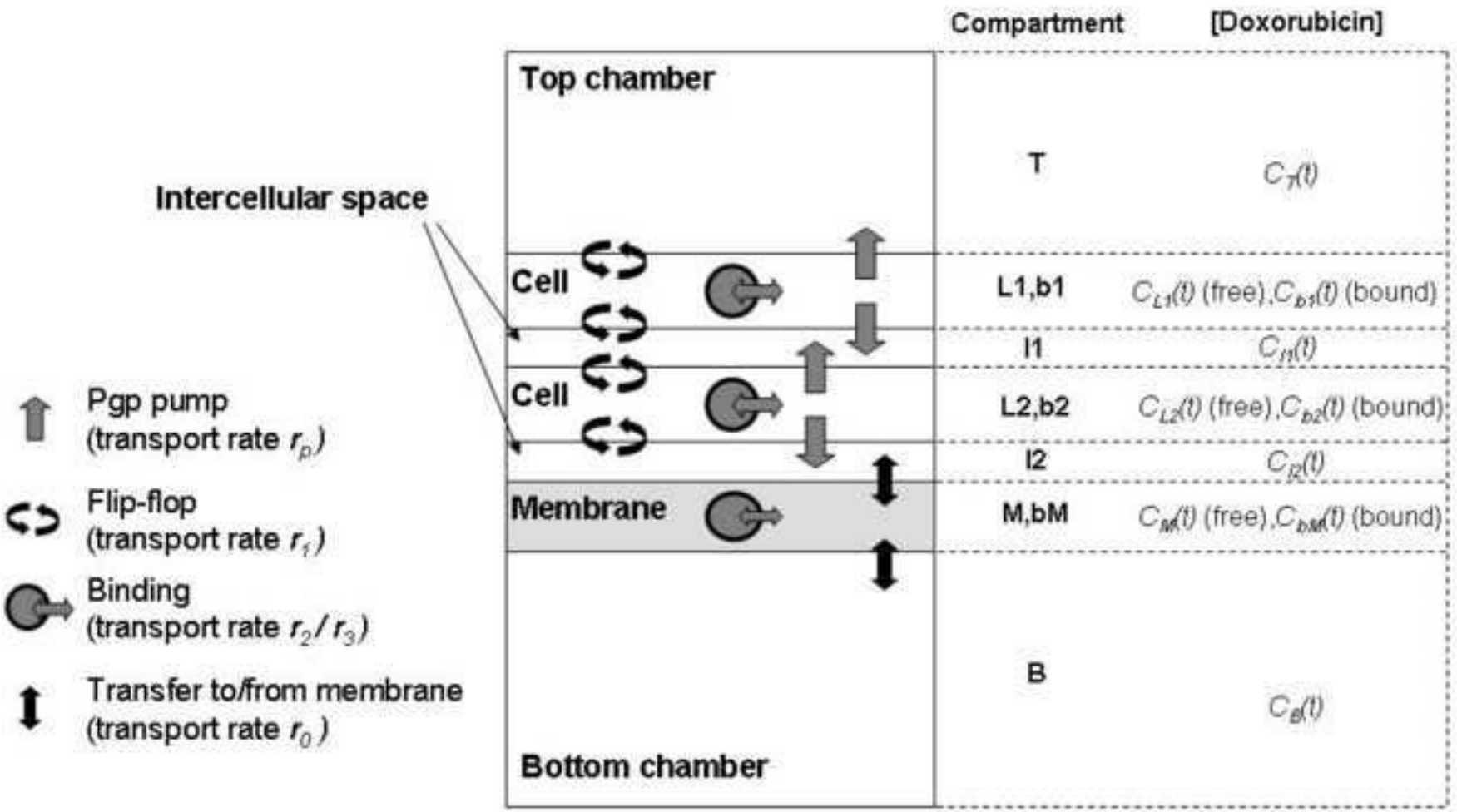

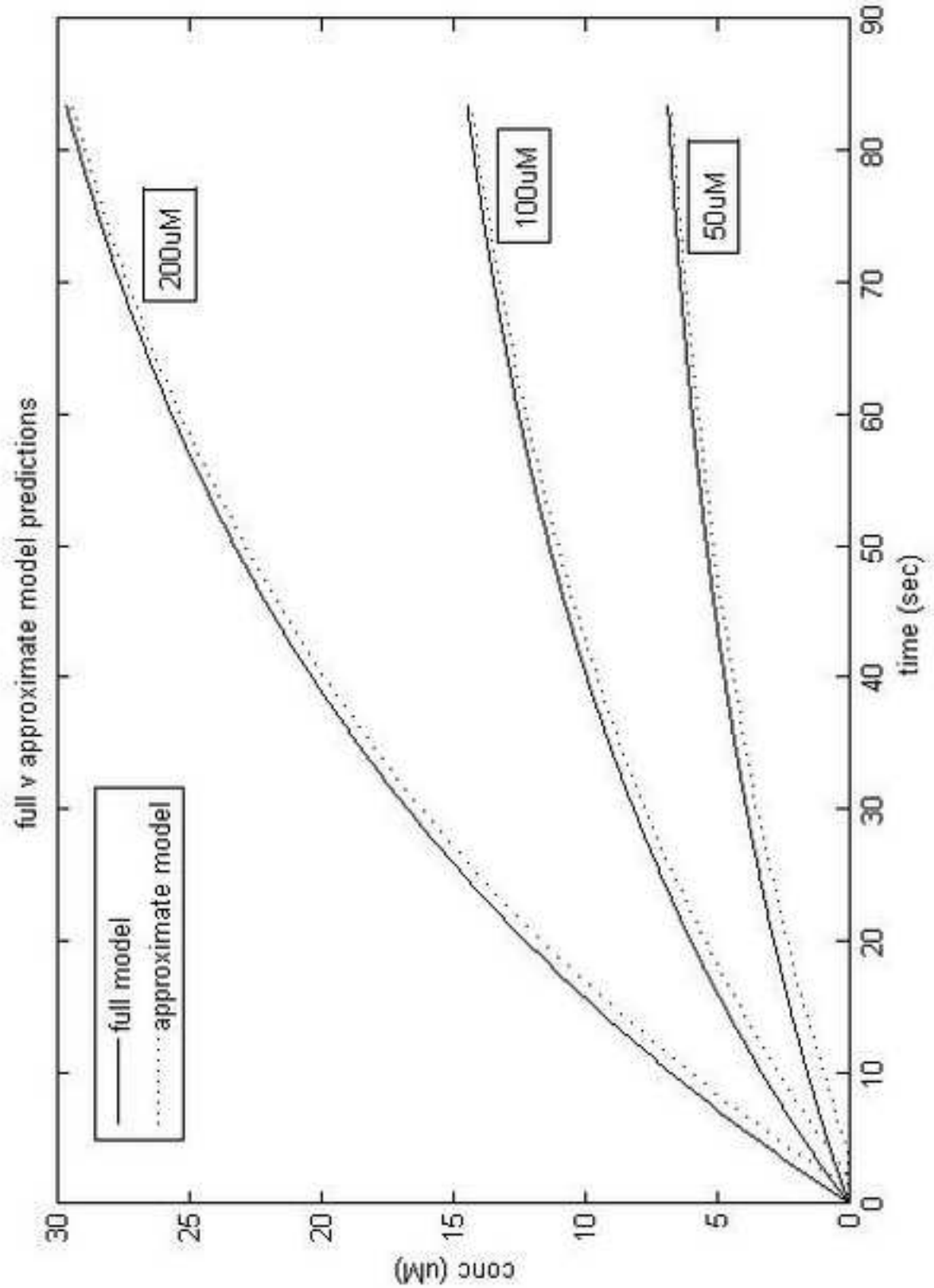

4. Figure 4

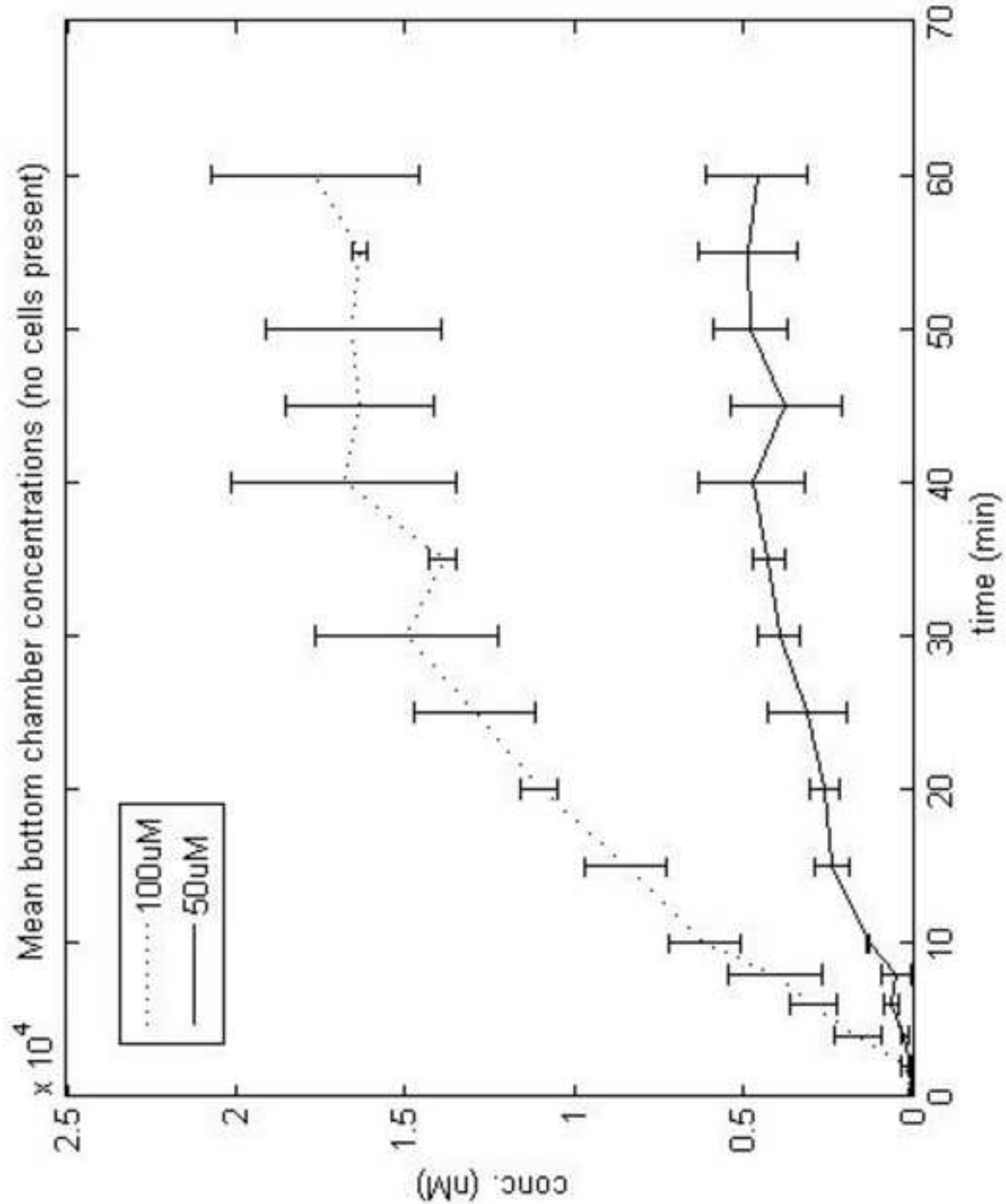

4. Figure 5

4. Figure 6

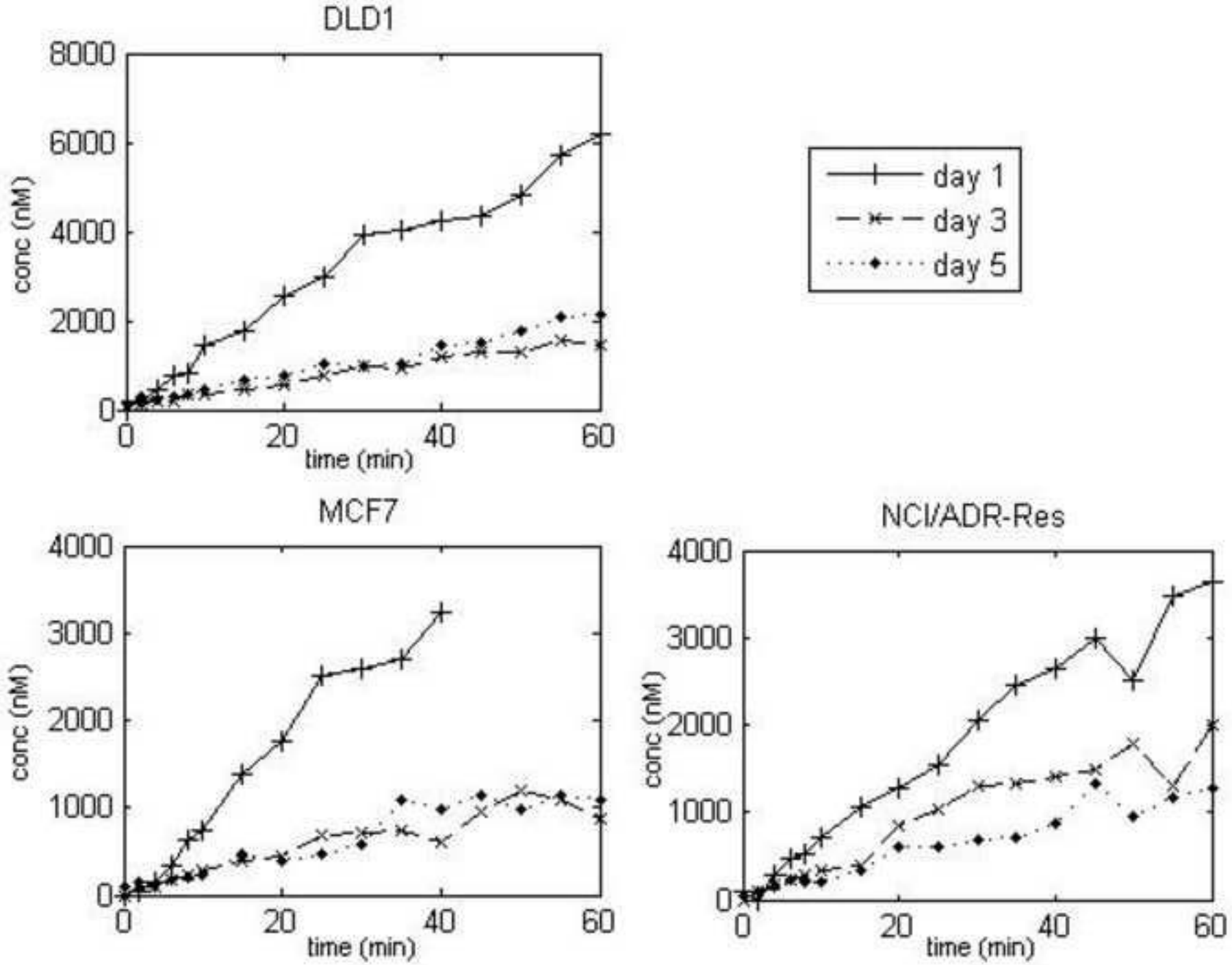

4. Figure 7

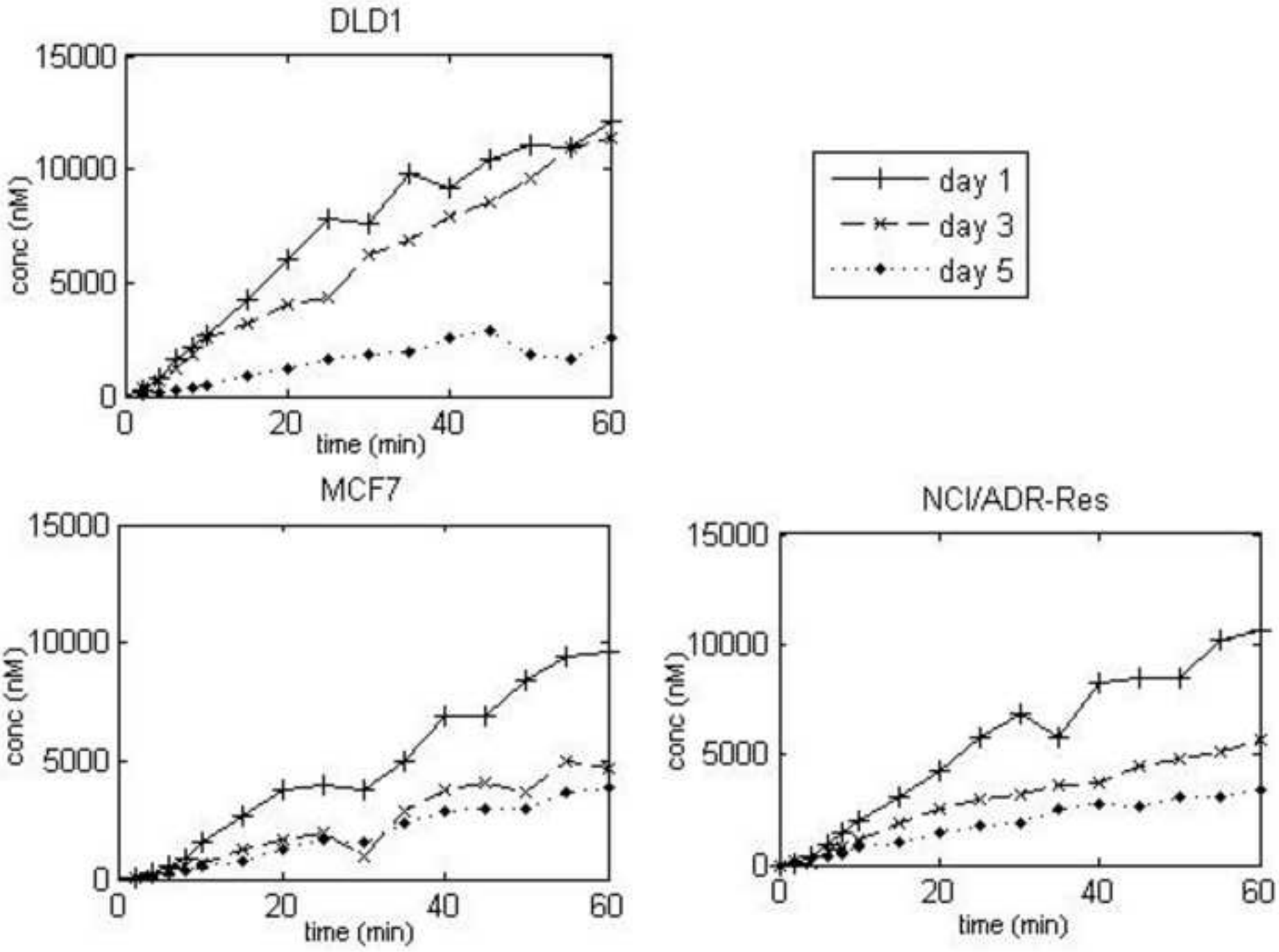

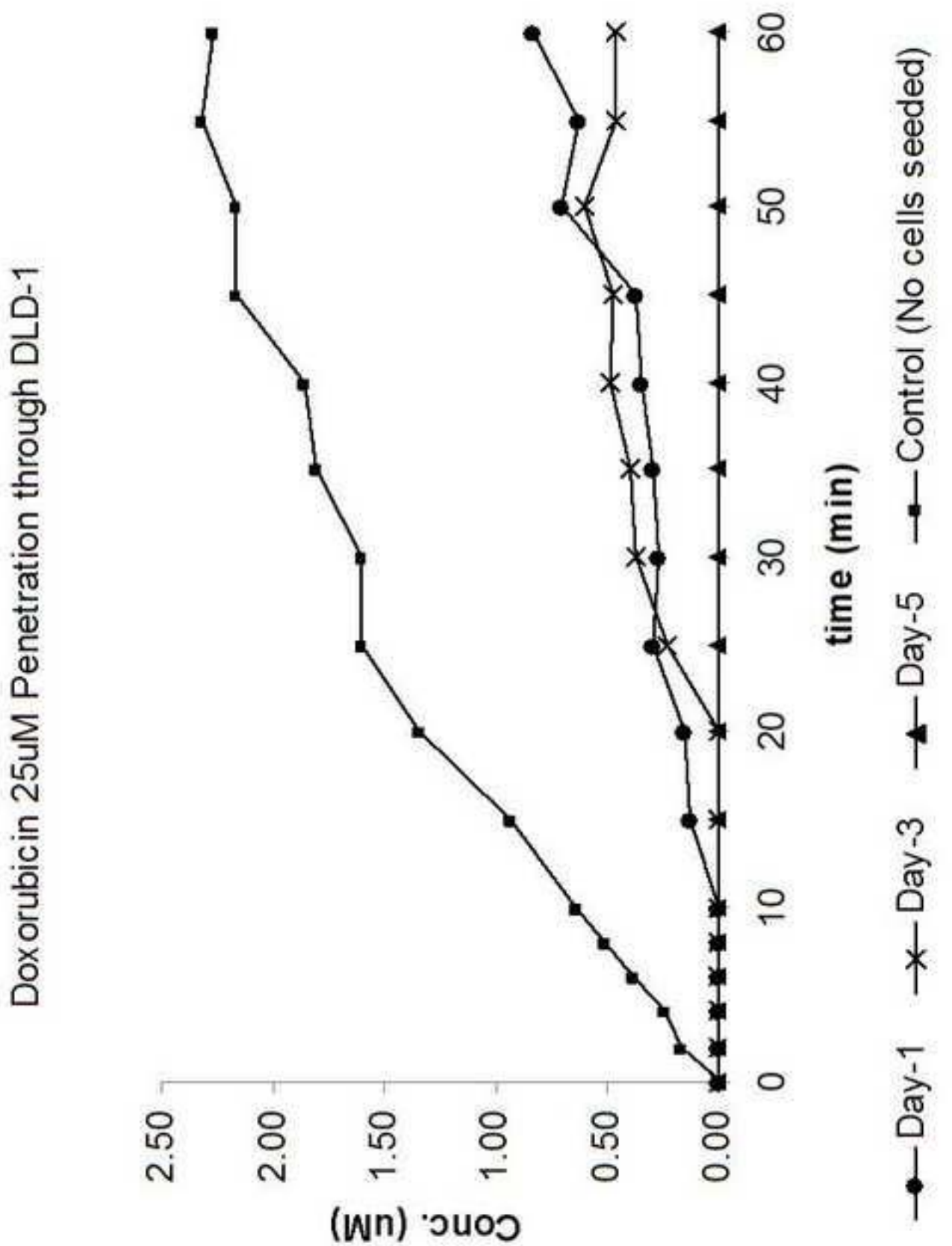

4. Figure 8

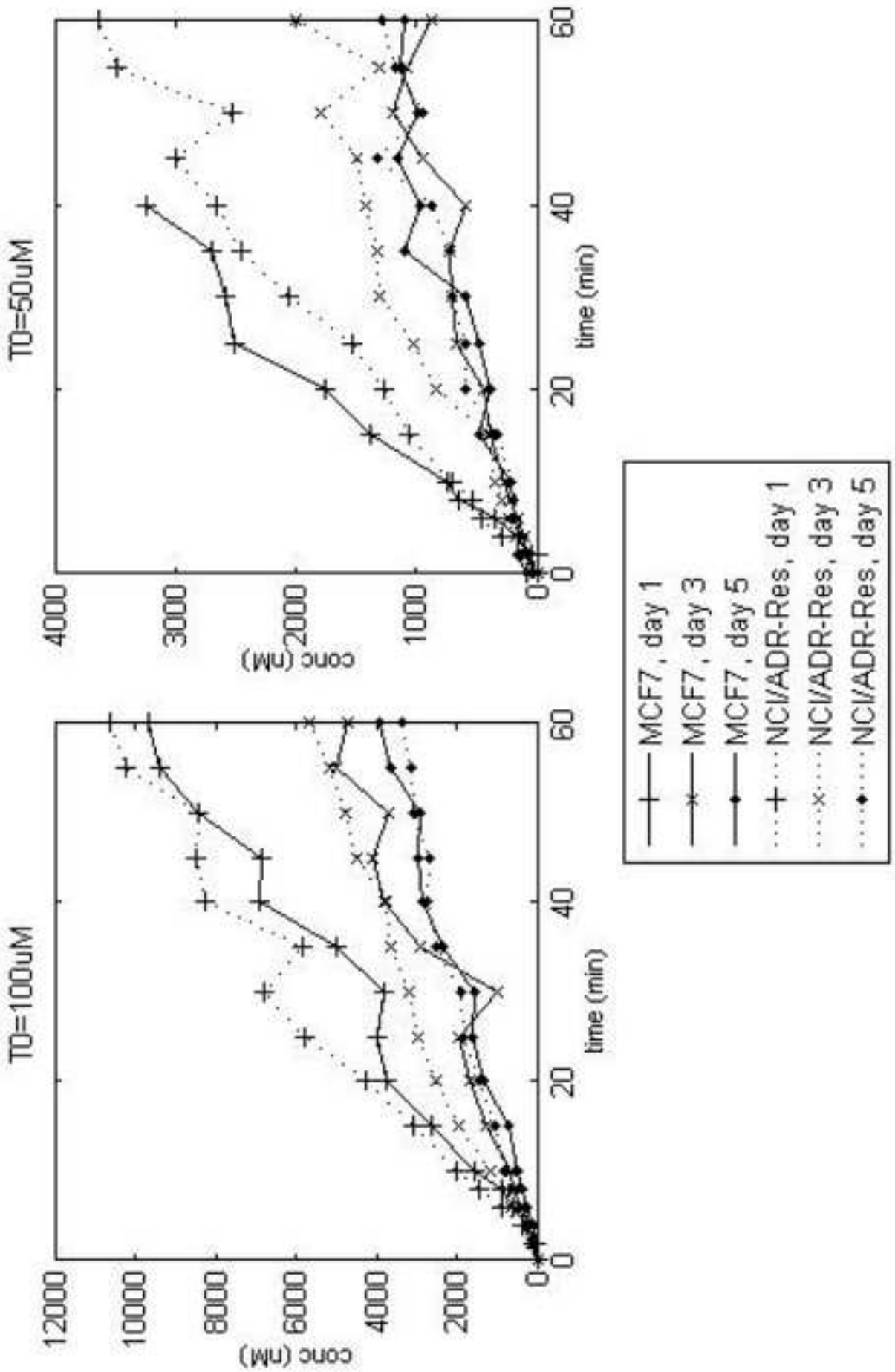

4. Figure 9

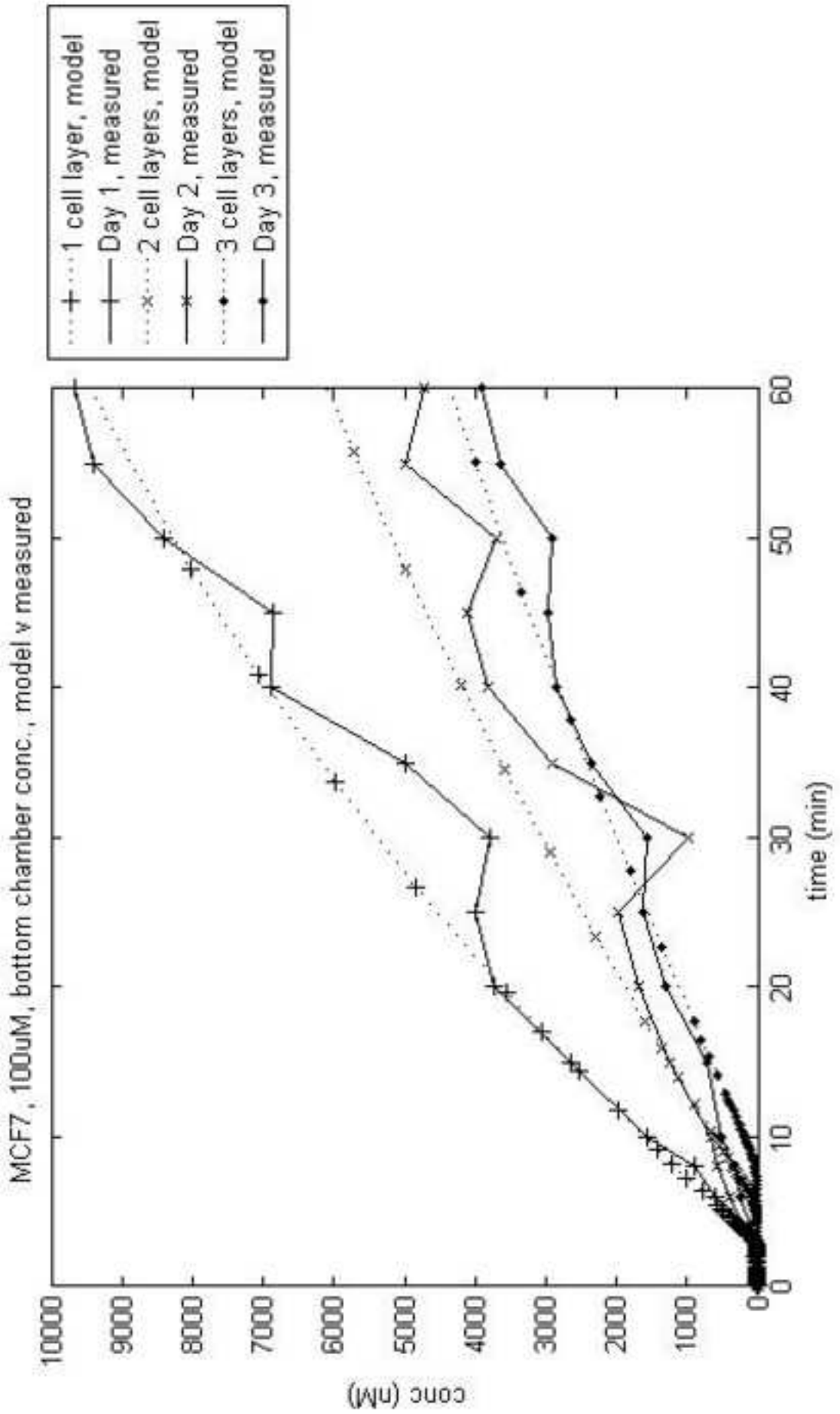

4. Figure 10

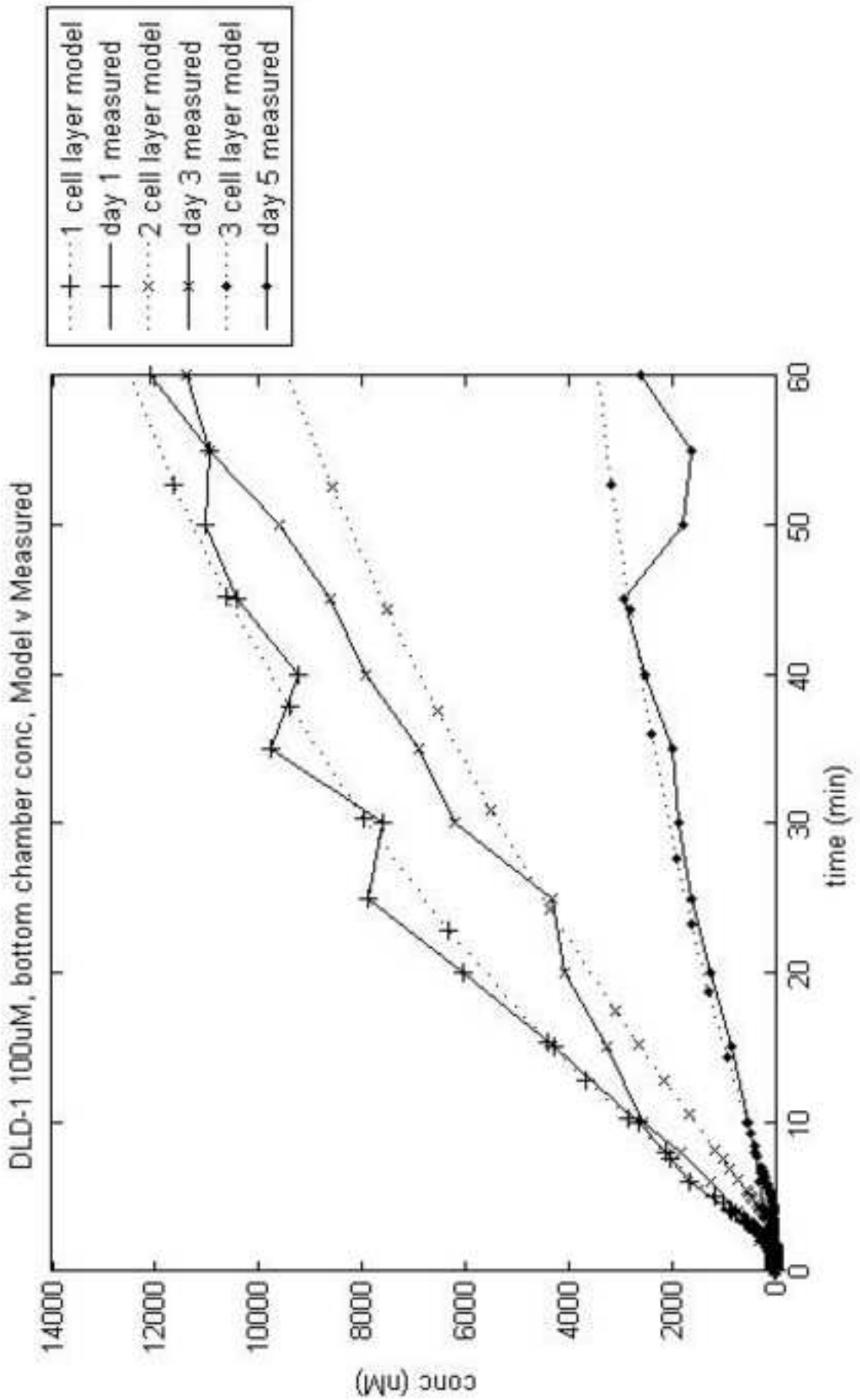

4. Figure 11

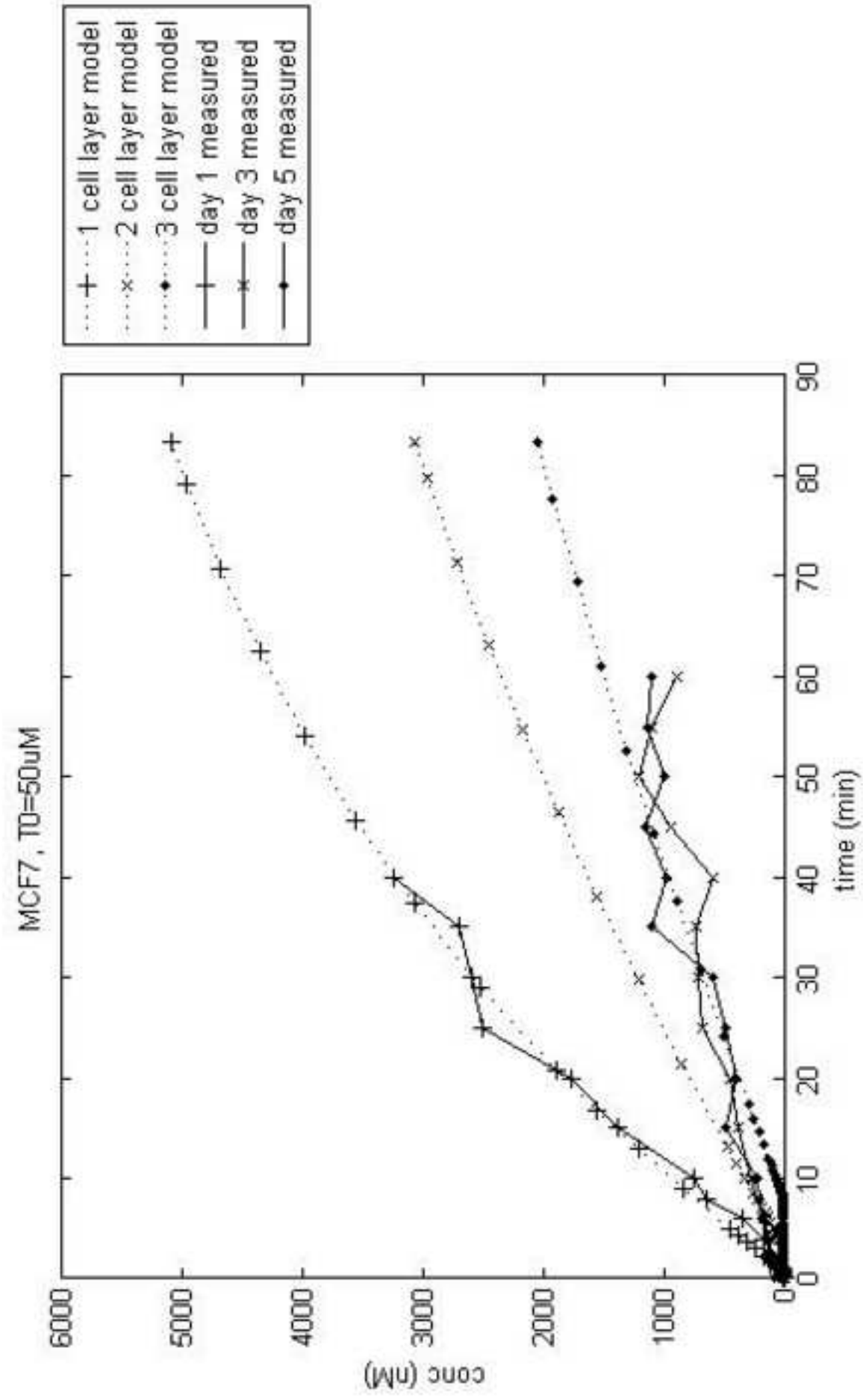

4. Figure 12

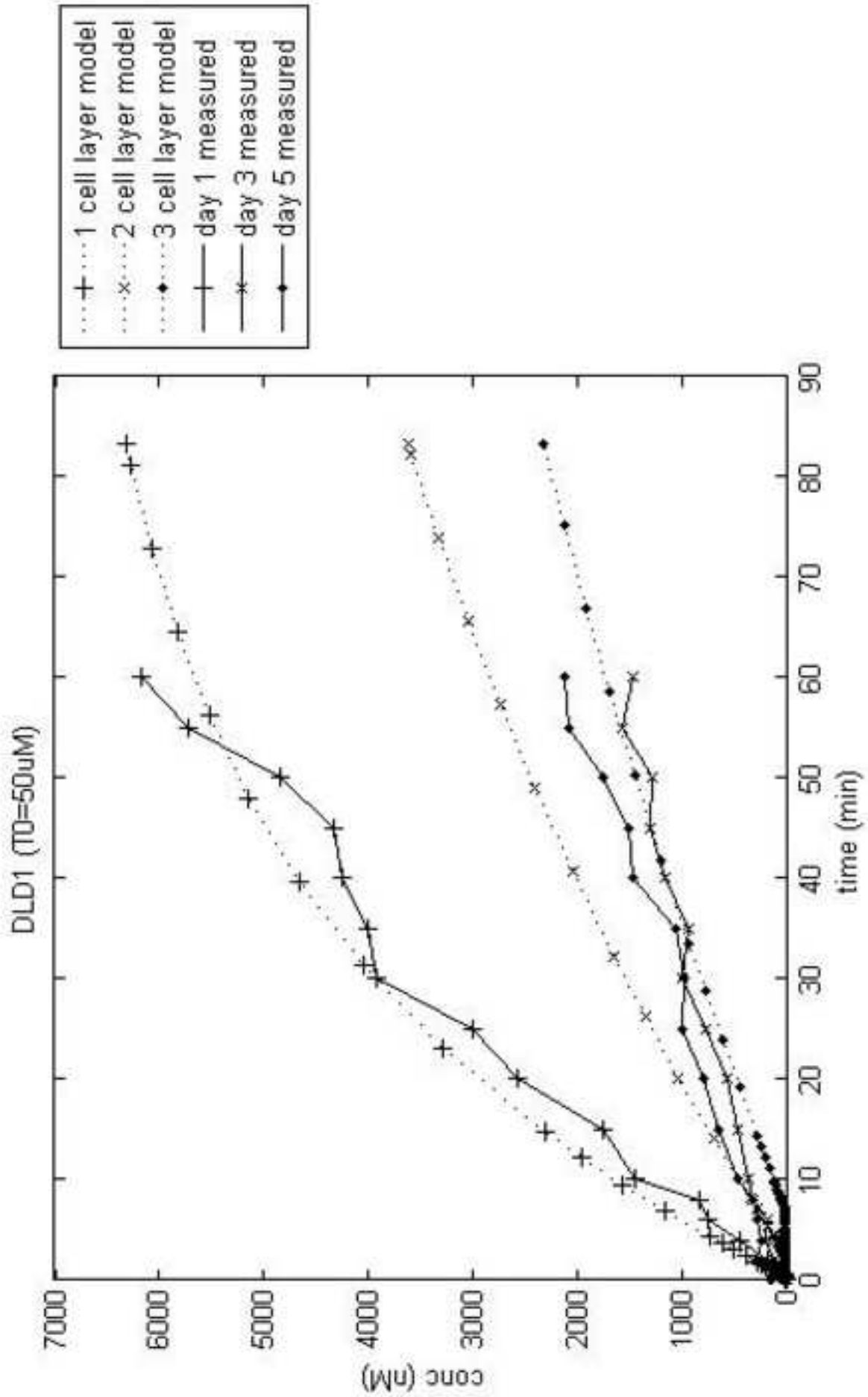

4. Figure 13